ADVANCED MATERIALS

www.advmat.de

Real-Time Observation of Carbon Nanotube Etching Process Using Polarized Optical Microscope

Qiuchen Zhao, Fengrui Yao, Zequn Wang, Shibin Deng, Lianming Tong, Kaihui Liu, and Jin Zhang**

Controllable synthesis of carbon nanotubes (CNTs) is of great importance in its further application, which attracts broad attention. As growth and etching are the two sides in the process of material crystallography and the control of the competition between them forms the foundation for modern technology of materials design and manufacture, the understanding on etching process of carbon nanotubes is still very unclear because technically it is of great challenge to characterize the dynamics in such small one-dimensional (1D) scale. Here the real-time investigation on the etching process of CNTs is reported, by the hot-wall chemical reactor equipped with a polarized optical microscope. It is discovered that the CNT etching behavior in air is totally of random, including the etching sites, termination sites, and structure dependence. Combining with the dynamic simulation, it is revealed that the random behavior reflects the unique "self-termination" phenomenon. A structure-independent etching propagation barrier of 2.4 eV is also obtained, which indicates that the etching propagation process still follows the conventional Kinetic Wulff construction theory. The results represent the new knowledge on the etching process in carbon nanotube and can contribute to its selective enrichment. Furthermore, the "self-termination" phenomenon may be a universal behavior in 1D process.

Etching process is regarded as one of the key points in selective enrichment of single-walled carbon nanotubes (SWNTs), including direct growth or post-treatment method.[1] However, though series of controlled trials strongly confirmed the existence of etching process, there is still a lack of theoretical direction in such an etching process in 1D carbon nanotube system. As we know, the crystal morphology evolution with time in 3D bulk materials has long been successfully described by Kinetic Wulff construction (KWC) theory,[2] which predicts that the kinetic growth and etching speed difference between different crystal facts determine the final materials shape.[3,4] Recently, KWC theory has also been applied to describe the morphology evolution in 2D atomic-layered materials, for example, graphene[5–7] and MoS_2.[8] However, as there is no "facet" definition, classical KWC model is hard to be directly used in describing 1D materials like carbon nanotubes. Could KWC theory be expanded to carbon nanotube etching process? What is the symptom like if it is applicative? Until now, the general understanding of the growth and especially etching behavior is still under its very immature stage, which to some extent hampers their accurate controllable growth.

To better understanding the etching process of 1D carbon nanotubes, many works had been published to observe this process by in situ observation methods at the level of individual SWNTs, including environmental transmission electron microscope,[9] environmental scanning tunneling microscope[10] or in situ Raman spectrum[11] . However, to quantitatively investigate the etching dynamics of intrinsic carbon nanotubes, it is prerequisite to see the nanotubes under etching condition in real-time (high time resolution at least on seconds level[10]) and identify their structure or chiral indices in situ (under high temperature up to 900 K). These commands are of great challenge due to the lack of the state-of-the-art technology to characterize nanotubes with very small diameter, which hampers the quantitative understanding in CNT etching process.[10–14]

In this report, we combined the high-throughput polarized optical microscope[15–17] with our hot-wall chemical reactor to fully cover the requirement to characterize the dynamics in nanotube etching process. The polarization microscope provides the unique capability of imaging individual nanotubes in real-time (frame rate up to 20 fpm) and identifying nanotube chiral indices in situ; while the hot-wall chemical reactor provides the high temperature (up to 1300 K) to initiate etching (**Figure 1**a). A short-wave pass filter was placed before the charge coupled device (CCD) camera to block the infrared black-body background radiation from hot reactor. SWNTs were grown directly onto a 3 mm × 4 mm silicon substrate with a 90 nm oxide layer (detailed characterization of SWNT samples

Q. C. Zhao, Z. Q. Wang, Dr. S. B. Deng, Prof. L. M. Tong, Prof. J. Zhang
Center for Nanochemistry
Beijing Science and Engineering Center for Nanocarbons
Beijing National Laboratory for Molecular Sciences (BNLMS)
College of Chemistry and Molecular Engineering
Peking University
Beijing 100871, China
E-mail: jinzhang@pku.edu.cn

F. R. Yao, Prof. K. H. Liu
State Key Laboratory for Mesoscopic Physics
School of Physics
Collaborative Innovation Center of Quantum Matter
Peking University
Beijing 100871, China
E-mail: khliu@pku.edu.cn

DOI: 10.1002/adma.201701959

© 2017 WILEY-VCH Verlag GmbH & Co. KGaA, Weinheim

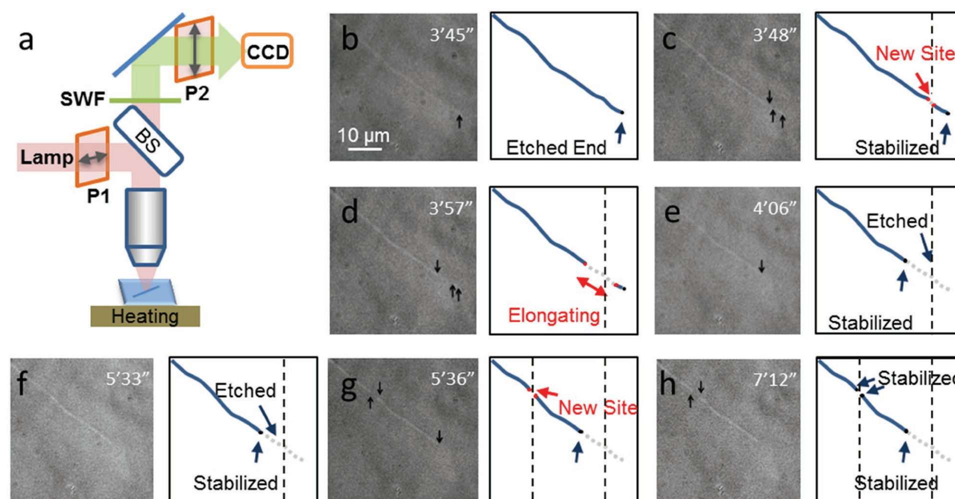

Figure 1. Instrument and typical results for in situ real-time monitoring etching process in carbon nanotubes. a) Scheme of combining high-contrast polarization microscopy with hot-wall reactor. A short-wave pass filter (SWF) is placed before the CCD to block the infrared black-body radiation. b–h) Key frames (left) and schematic illustrations (right) of etching evolution in one nanotube. Vertical black dashes point out the initial etching sites, gray dashes indicate the etching gap, and red (black) point refers to active (inactive) etching sites.

are shown in Figure S1, Supporting Information). After placing the as-grown samples into the reactor, we monitored the etching process of each carbon nanotube by taking video on them. As shown in Section SI 2 (Supporting Information), our as-grown SWNT samples is longer than 2 mm, and we simply chose tens of micrometers in the middle it, which ensure that the etching process is generated from the body of the SWNT. One example of the etching evolution is shown in Figure 1b–h with time interval of 3 s (schemes were also shown for clear illustration). At 3′45″, the nanotube etching stops (Figure 1b, the former morphology of this carbon nanotube is in Figure S1, Supporting Information), and 3 s later a new etching site appears (Figure 1c) and the gap gradually elongates to about 10 µm in the following 18 s (Figure 1c–e). Quite interestingly, the etching site stops again (Figure 1e,f) until a new etching site appears at a new position (Figure 1g) and it starts another circle of this "new site-elongation-termination-new site" (Figure 1g,h). Our real-time observation highlighted the phenomenon in nanotube etching process that the etching proceed in an unexpected way: new etching sites appear along the CNT, every etching site introduces a finite but nonconstant gap, and every etching site will terminate (These results are in sharp contrast to previous understanding of continuous[12–14] or semicontinuous segment-by-segment[10] etching process that starts from the nanotube end, which were obtained based on observation without real-time imaging of the etching dynamics). It is true that limited by the optical diffraction limitation, we could not give a higher spatial resolution for the position of the ends. However, the etching rate in Figure 1c–e (≈0.5 µm s^{-1}) is much larger than the etching rate in Figure 1e–h (which do not show a observable change in 3 min), a significant reduction of etching rate by at least three orders of magnitude folds took place during the etching process, which could be regarded as terminated in our observation time scale. Considering that the residual catalyst nanoparticles or substrates may lead to the etching of SWNTs, we annealed the as-grown samples in protection of Ar at the same temperature for 1 h, while no etching phenomenon is observed, which could strongly verify that the etching process is dominated by air.

In order to quantitatively understand the random etching evolution behavior in carbon nanotubes, we carried out statistic study along different nanotubes with typical length of more than 4 mm. **Figure 2**a–c shows the typical results along one carbon nanotubes under different etching time of 5, 10, and 20 min respectively (more experimental details are given in Figure S3, Supporting Information). For the convenience of description, we defined several parameters along the nanotubes in Figure 2d, where l_k refers to the length of kth segment of nanotube (marked as S_k), and d_k denotes the gap length between S_k and S_{k+1} segment (marked as G_k). We first statistically measured the distance (defines as $\frac{1}{2}(d_k+d_{k+1})+l_{k+1}$) between G_k and G_{k+1} for 100 gaps (etching time $t = 5$ min unless specially mentioned in below), which reflects the distance distribution of neighboring etching sites. The significant variation of this distance showed that the new etching sites start at random positions (Figure 2e). We claimed that the random etching site is related to the ideal structure of the as-grown SWNT samples, which do not have defects on the body of SWNTs (more evidences are shown in Figure S3, Supporting Information). The uniform structure along the carbon nanotube makes the probability of etching site generation equally, which lead to the random behavior of the position of etching site. We further plot the statistics of gap length d_k (Figure 2f), which reflects the elongation ability of each active site. The gap length distributions are of nonconstant and conform to a Gaussian-like distribution. We last plot the remnant nanotube ratio (defined as $L/L_0, L=\sum_k l_k,\ L_0=\sum_k (l_k+d_k)$) under different etching time (Figure 2g). Quite strangely, the etching rate decays gradually over time and shows a saturate behavior. This saturation behavior is quite contradictory to the perdition in classic 3D

© 2017 WILEY-VCH Verlag GmbH & Co. KGaA, Weinheim

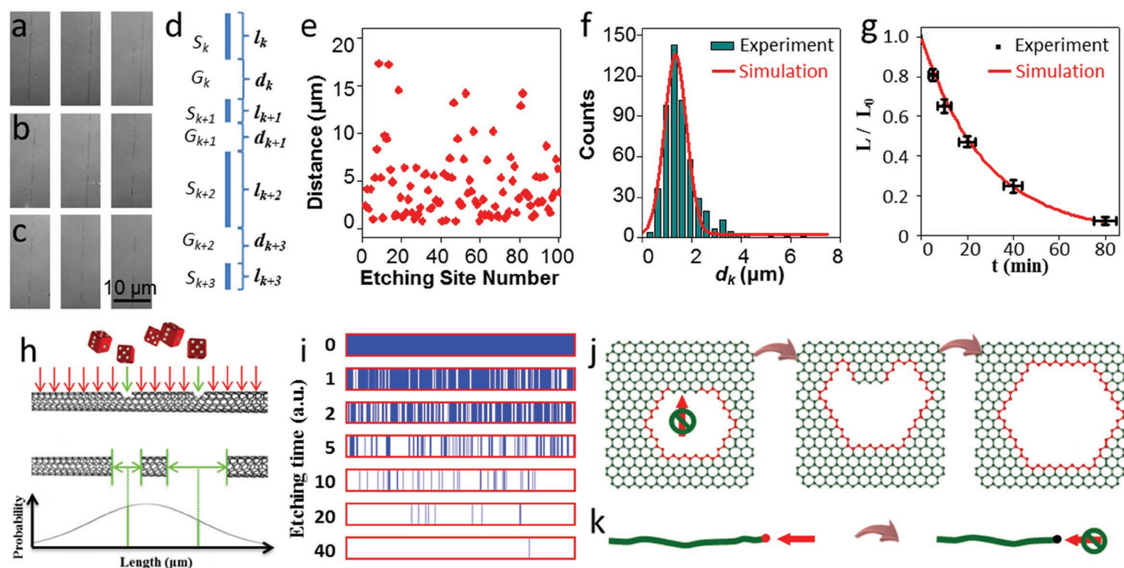

Figure 2. Dynamic behavior and modeling of SWNT etching process. Optical imaging of SWNT segments with etching time of a) 5 min, b) 10 min, and c) 20 min. d) Definition of the segment/gap number and their length. e) Distance of the neighboring gaps. f) Experiment result and simulation of gap length distribution after 5 min etching. g) Experiment result and simulation of relative length of remnant SWNT over time. h) Schematic illustration of random etching process. i) Simulated evolution of SWNT over etching time. Blue ribbons refer to remained SWNT segments S_k and white blanks are the etched gaps G_k. j–k) Comparison of the different etching behavior in 2D and 1D systems. The red sites are the active sites during etching process.

or 2D materials, where the etching will not terminate and the etching rate is of constant (without new site production) or an accelerating value (with new site production).

To better understanding the above etching process, we developed a phenomenological 1D etching model and simulated the entire etching process (schematically illustrated in Figure 2h). The key setting in our model is the random appearance and the termination of etching sites. Other technical details include that the active etching site is produced at a random point with a frequency τ_0, and the gap length is determined by a random number generator with Gaussian function (see details in Figures S7–S9, Supporting Information). The simulated results of nanotube segment evolution are shown in Figure 2i, in which blue ribbons refer to S_k segments and the white parts are the gaps G_k. The simulated d_k distribution and time evolution of L/L_0 nicely reproduce our experimental results in Figure 2f,g (simulated results are shown by the red curves).

From both our experimental and simulation results, we revealed that the crucial difference between carbon nanotube and other higher dimensional materials lies in the existence of etching termination sites. Herein, we used carbon nanotube and graphene as a contrast to explain this unique difference induced by dimensionality (Figure 2j,k). During the etching process, the number of active site shows a positive correlation with the etching time. When some etching sites become inactive in graphene, etching could sustain at neighboring active sites. During further etching process, the inactive sites could be attacked from other directions and entirely removed. Thus, the self-termination behavior does not have much impact on the overall etching process. However, in carbon nanotube etching process, the active etching site did not change over time (the cylinder structure makes the cross sectional area of the SWNT remains unchanged during etching process, which is the main difference between SWNT and graphene). Thus, the inactive sites could not be surpassed from other routes due to the 1D confinement. Therefore the self-termination is a unique characteristic in the etching process of carbon nanotube to form other carbon materials. Furthermore, as the side reactions are ubiquitous in chemical reactions, we claimed that the "self-termination" process should be a universal phenomenon 1D system.

The advanced ability of our equipment of in situ chirality identification enables us to investigate the structure dependence of the etching behavior in 1D nanotubes. The chiral indices were obtained by comparing the optical transition energies in the optical spectrum to the atlas table we established before.[15,16,18,19] One example of a semiconducting (15, 13) tube is given in **Figure 3**a. We measured the etching gap size d_k at different etching sites on this nanotube and found that they show Gaussian-like random distribution with average value $\overline{d_k}$ of 1.0 μm (Figure 3b), which reflects the etching propagation ability. We statistically studied the chirality dependence of this etching gap behavior (under the same etching time and heating temperature) and found that there is no obvious differences between different nanotubes (Figure 3c), no matter they are semiconducting or metallic (diameter in the range 1.3–2.8 nm). Here we noted that unlike the previous studies that involve nanotube transferring process, all characterizations were carried out on as-grown samples and the obtained properties are related to the intrinsic nanotube properties. Though it was widely held in belief that the etching is highly related to the nanotube structures,[20–25] the chirality-independent etching gap meant that the etching propagation process remains the same for different kinds of nanotubes. This nonselective propagation process strongly suggested that a uniform structure could form during etching process (for example, an armchair[26] or zigzag[27] ends are mostly possible according to previous reports), which

© 2017 WILEY-VCH Verlag GmbH & Co. KGaA, Weinheim

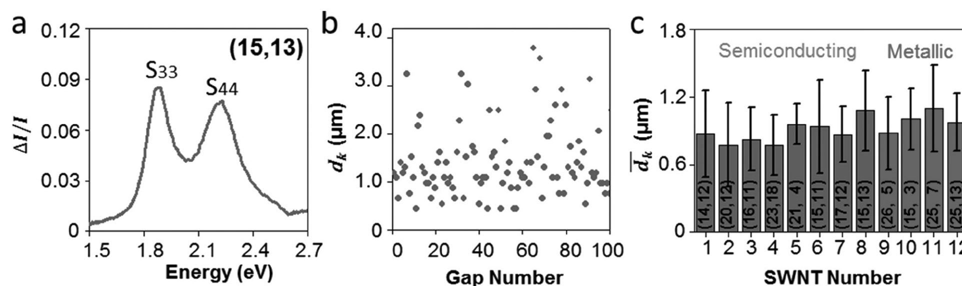

Figure 3. Structure-independent etching propagation behaviors in SWNTs. a) Typical optical spectroscopy of a (15, 13) tube, which is a semiconducting SWNT with the diameter of 1.9 nm. b) Etching gap length of the (15, 13) tube after a 5 min etching. In total 100 gaps have been measured with the average length of 1.1 ± 0.4 µm. c) Relationship between average gap lengths and SWNT chiralities. Although selected SWNTs have different diameter (1.3–2.8 nm), helix angle (8°–28°), and electronic types, the average gap lengths are very similar.

does not vary over nanotube structure. Regarding this uniform structure as a special "facet," the etching behavior could also be well described by KWC model before termination process. As KWC had been proved to be applicable in the etching process of 2D materials,[5–8] it is the first time to observe the KWC behavior in 1D carbon nanotube etching process.

Now we provided a full picture to describe the random etching behavior in 1D carbon nanotube systems. A polymerization-like mechanism, including initiation, propagation, and termination process, was utilized to illustrate the dynamic mechanism of etching process. The etching site initiation, etching propagation, and etching site termination are all ruled by the activation energy barrier (**Figure 4**a). From the fact that the termination is the most stable and the propagation is the most possible event, we know that termination barrier (ΔE_t) > initiation barrier (ΔE_i) > propagation barrier (ΔE_p). The initiation barrier could be obtained in analogy with graphene etching process with an energy gap $\Delta E_i \approx 2.7$ eV,[28] which at first forms an epoxy group. The epoxy groups formed during oxidation were suggested to have a preference for aligning in a line based on first-principles calculation, which induced a rupture of the underlying C–C bonds. An epoxy pair could form during the deeper oxidation and then a more stable carbonyl pair could form. Finally, carbon nanotubes could be clipped into two parts with zigzag ends with carbonyl structures.[27] The propagation barrier ΔE_p can be obtained from the temperature-dependent gap length data (Figure 4b). This energy gap leads to a tunneling process probability p in a unit interval. Thus, the average length of the gap $\overline{d_k}$ should be proportional to etching probability p. Since p is related to the energy ΔE_p in the relation of $p = A\exp(-\Delta E_p / k_B T)$, we obtained

$$\ln \overline{d_k} = -\frac{\Delta E_p}{k_B} \cdot \frac{1}{T} + C \tag{1}$$

where k_B is Boltzmann constant, C is a constant related to the reaction type and T refers to the etching temperature. The obtained ΔE_p from our data is ≈2.4 eV (Figure 4c), which is about 0.3 eV lower than ΔE_i. Finally we discuss the largest termination barrier ΔE_t, from which we know the edge structure is very stable even in air under high temperature around 900 K. Due to the lack of characterization methods, we still know little about the mechanism and atomic structure for this termination edge. As known that the etching of a CNT is very sensitive to the end structure (for example, the activity of open or closed ends are significantly different), we also believed that the termination is caused by the sudden variation of the end structure. This variation may be an inherent side reaction in the reaction of CNT and O_2, or due to the complex interaction between carbon nanotube ends and substrates. The nature in the end structure deserves the detailed study in the near future.

With in situ real-time observation, we observed the etching process of carbon nanotube. We found that KWC model is still applicable in describing the propagation stage during etching process in 1D carbon nanotubes. However, a self-termination beyond KWC model must be included, which is a unique characteristic for carbon nanotubes due to its reduced dimension. These findings should provide new insights in the design of carbon nanotubes and facilitate its controllable growth, such as chirality-enrichment growth. Besides, the special phenomenon of self-termination may also be used widely in other etching process of other 1D material, like 1D polymer chains.

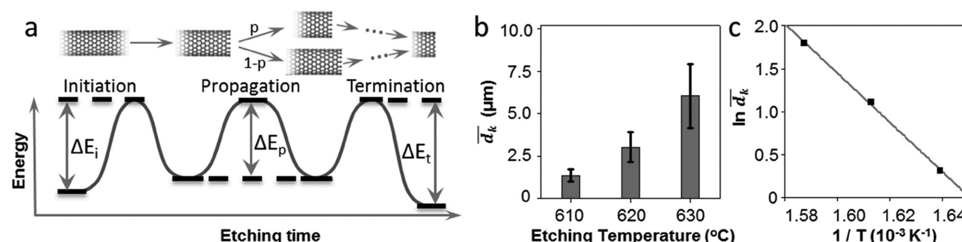

Figure 4. Mechanism of SWNT etching process. a) Schematic illustration of the three steps in SWNT etching process. The etching process is ruled by initiation barrier (ΔE_i), propagation barrier (ΔE_p) and termination barrier (ΔE_t). b) Average gap length under different etching temperature with the etching time of 5 min. c) linear fitting of $\ln\overline{d_k} - T^{-1}$. An etching propagation energy barrier of 2.4 eV is obtained.

© 2017 WILEY-VCH Verlag GmbH & Co. KGaA, Weinheim

Experimental Section

Growth of Flow Direct SWNT Arrays: Carbon nanotubes were grown in chemical vapor deposition (CVD) system. In particular, 3 mm × 4 mm SiO_2/Si wafers with 90 nm oxide layer (Hefei Kejing Materials Technology Company, China) were used as substrates. $Fe(OH)_3$/ethanol sol, as catalyst precursor, was dispersed onto a prepositive substrate on the upstream of gas flow. Substrates were heated to 980 °C in the air in 50 min, and then the CVD system was purged with 200 sccm argon for 10 min. After that, a flow of hydrogen (100 sccm) and argon (through an ethanol bubbler with 50 sccm) was introduced for the growth of SWNTs at the same temperature for 15 min. A programmed cooling process was operated from 980 to 830 °C in 60 min with the protection of 100 sccm H_2 and then natural cooling to room temperature.

Polarized Optical Imaging of Individual SWNT: As shown in Figure 1a, an optical microscope (Olympus BX51) equipped with a 50 × objective (N.A. = 0.5, working distance of 1.06 cm), two polarizers (Daheng optics, GCL-050003), a short-wave pass filter <610 nm (Thorlabs, FGB 37), and a monochrome camera (Andor Zyla 4.2) were used to image the carbon-nanotube in situ. A tungsten–halogen lamp was used as the light source, the reflective mode was used, one polarizer was located in the incident beam with its transmission axis set horizontally, and the second polarizer was placed in the reflective beam with its transmission axis set to a small angle θ from the vertical direction. A Kohler illuminator provided evenly dispersed light across the plane of field of view. The aperture iris diaphragm and the field iris diaphragm enabled convenient controls of incident beam.

In Situ Observation of SWNT Etching: The as-grown SWNTs substrates were placed into hot-wall reactor exposed in atmospheric phenomenon. The samples were heated up to target temperature with 100 °C min^{-1}. The etching process was monitored by real-time video mode.

Chirality Assignment of As-Grown SWNT: The home-built single-tube high-contrast reflection spectroscopy employed a supercontinuum laser as light source and a spectrometer as photon energy analyzer. The optical transition energies was used to determine the chirality of each nanotube.[18,29]

Supporting Information

Supporting Information is available from the Wiley Online Library or from the author.

Acknowledgements

This work was supported by the National Natural Science Foundation of China (21233001, 21129001, 51272006, 51432002, 51121091, 51522201, and 11474006) and the National Key R&D Program of China (2016YFA0200101, 2016YFA0200104, and 2016YFA0300903).

Conflict of Interest

The authors declare no conflict of interest.

Keywords

carbon nanotubes, etching, in situ observation

Received: April 7, 2017
Published online: June 6, 2017

[1] C. Liu, H.-M. Cheng, *J. Am. Chem. Soc.* **2016**, *138*, 6690.
[2] G. Wulff, *Z. Krystallogr. Mineral.* **1901**, *34*, 449.
[3] R. F. Sekerka, *Cryst. Res. Technol.* **2005**, *40*, 291.
[4] E. Auyeung, T. Li, A. J. Senesi, A. L. Schmucker, B. C. Pals, M. O. de la Cruz, C. A. Mirkin, *Nature* **2014**, *505*, 73.
[5] R. Yang, L. C. Zhang, Y. Wang, Z. W. Shi, D. X. Shi, H. J. Gao, E. G. Wang, G. Y. Zhang, *Adv. Mater.* **2010**, *22*, 4014.
[6] T. Ma, W. C. Ren, X. Y. Zhang, Z. B. Liu, Y. Gao, L. C. Yin, X. L. Ma, F. Ding, H. M. Cheng, *Proc. Natl. Acad. Sci. USA* **2013**, *110*, 20386.
[7] M. Lukas, V. Meded, A. Vijayaraghavan, L. Song, P. M. Ajayan, K. Fink, W. Wenzel, R. Krupke, *Nat. Commun.* **2013**, *4*, 1379.
[8] M. Yamamoto, T. L. Einstein, M. S. Fuhrer, W. G. Cullen, *J. Phys. Chem. C* **2013**, *117*, 25643.
[9] A. L. Koh, E. Gidcumb, O. Zhou, R. Sinclair, *ACS Nano* **2013**, *7*, 2566.
[10] H. A. Mehedi, J. Ravaux, K. Yazda, T. Michel, S. Tahir, M. Odorico, R. Podor, V. Jourdain, *Nano Res.* **2016**, *9*, 517.
[11] A. Li-Pook-Than, J. Lefebvre, P. Finnie, *ACS Nano* **2013**, *7*, 6507.
[12] P. M. Ajayan, T. W. Ebbesen, T. Ichihashi, S. Iijima, K. Tanigaki, H. Hiura, *Nature* **1993**, *362*, 522.
[13] S. C. Tsang, P. J. F. Harris, M. L. H. Green, *Nature* **1993**, *362*, 520.
[14] J. T. Ye, Z. K. Tang, *Phys. Rev. B* **2005**, *72*, 045414.
[15] K. H. Liu, X. P. Hong, Q. Zhou, C. H. Jin, J. H. Li, W. W. Zhou, J. Liu, E. G. Wang, A. Zettl, F. Wang, *Nat. Nanotechnol.* **2013**, *8*, 917.
[16] S. B. Deng, J. Y. Tang, L. X. Kang, Y. Hu, F. R. Yao, Q. C. Zhao, S. C. Zhang, K. H. Liu, J. Zhang, *Adv. Mater.* **2016**, *28*, 2018.
[17] K. Liu, F. Yao, C. Chen, C. Liu, J. Zhang, F. Wang, *Chem. - Eur. J.* **2017**.
[18] K. H. Liu, J. Deslippe, F. J. Xiao, R. B. Capaz, X. P. Hong, S. Aloni, A. Zettl, W. L. Wang, X. D. Bai, S. G. Louie, E. G. Wang, F. Wang, *Nat. Nanotechnol.* **2012**, *7*, 325.
[19] K. Liu, X. Hong, S. Choi, C. Jin, R. B. Capaz, J. Kim, W. Wang, X. Bai, S. G. Louie, E. Wang, F. Wang, *Proc. Natl. Acad. Sci. USA* **2014**, *111*, 7564.
[20] G. Y. Zhang, P. F. Qi, X. R. Wang, Y. R. Lu, X. L. Li, R. Tu, S. Bangsaruntip, D. Mann, L. Zhang, H. J. Dai, *Science* **2006**, *314*, 974.
[21] B. Yu, C. Liu, P. X. Hou, Y. Tian, S. S. Li, B. L. Liu, F. Li, E. I. Kauppinen, H. M. Cheng, *J. Am. Chem. Soc.* **2011**, *133*, 5232.
[22] B. Yu, P. X. Hou, F. Li, B. L. Liu, C. Liu, H. M. Cheng, *Carbon* **2010**, *48*, 2941.
[23] Y. Miyata, T. Kawai, Y. Miyamoto, K. Yanagi, Y. Maniwa, H. Kataura, *J. Phys. Chem. C* **2007**, *111*, 9671.
[24] E. Borowiak-Palen, T. Pichler, X. Liu, M. Knupfer, A. Graff, O. Jost, W. Pompe, R. J. Kalenczuk, J. Fink, *Chem. Phys. Lett.* **2002**, *363*, 567.
[25] S. Nagasawa, M. Yudasaka, K. Hirahara, T. Ichihashi, S. Iijima, *Chem. Phys. Lett.* **2000**, *328*, 374.
[26] T. W. Odom, J. L. Huang, P. Kim, C. M. Lieber, *J. Phys. Chem. B* **2000**, *104*, 2794.
[27] Z. Y. Li, W. H. Zhang, Y. Luo, J. L. Yang, J. G. Hou, *J. Am. Chem. Soc.* **2009**, *131*, 6320.
[28] J. L. Li, K. N. Kudin, M. J. McAllister, R. K. Prud'homme, I. A. Aksay, R. Car, *Phys. Rev. Lett.* **2006**, *96*, 176101.
[29] F. R. Yao, J. Y. Tang, F. Wang, K. H. Liu, *J. Opt. Soc. Am. B* **2016**, *33*, C102.

© 2017 WILEY-VCH Verlag GmbH & Co. KGaA, Weinheim